This is the Author Accepted Manuscript (postprint) version of the following paper:
Daniela Caschera, Roberta Grazia Toro, Fulvio Federici, Roberta Montanari, Tilde deCaro , Mona T. Al-Shemy, Abeer M. Adel Green approach for the fabrication of silver-oxidized cellulose nanocomposite with antibacterial properties (2020) peer-reviewed and accepted for publication in Cellulose, https://doi.org/10.1007/s10570-020-03364-7(0123456789© <2020>.
Springer Nature B.V. 2020
This manuscript version is made available under the CC-BY-NC-ND 4.0 license https://creativecommons.org/licenses/by-nc-nd/4.0/

Manuscript

Click here to view linked References

Click here to download Manuscript
Manuscript_revised_def.docx

Green approach for the fabrication of silver-oxidized cellulose nanocomposite with antibacterial properties

Daniela Caschera[a*], Roberta Grazia Toro[a], Fulvio Federici[a], Roberta Montanari[b], Tilde de Caro[a], Mona T. Al-Shemy [c], Abeer M. Adel[c]

[a] Institute for the Study of Nanostructured Materials, ISMN-CNR, Via Salaria km 29,300 Monterotondo, Rome, Italy

[b] Institute of Crystallography, IC-CNR, Via Salaria Km 29,300, Monterotondo, Rome, Italy

[c] National Research Centre, Cellulose and Paper Department, 33El-Bohouth St. (Former El-Tahrir St.), Dokki, P.O. 12622, Giza, Egypt

* Corresponding author

daniela.caschera@cnr.it

Phone: +39 0690672848

Acknowledgments

The authors thank Mrs. Luciana Cerri for her technical assistance in AFM analysis, Marianna Barbalinardo for SEM measurements and Mr. Claudio Veroli for the XRD measurements. The activities have been performed in the framework of the Joint Bilateral Agreement CNR/NRC (Italy/Egypt), Biennial Programme 2018-2019, for the project “Improvement of mechanical and barrier properties of biopolymer nano-composites for packaging applications”.

Abstract

Herein we present facile and green two-steps method for the fabrication of silver-carboxylated nanocellulose (Ag-ONCs) nanocomposite. Respecting the Circular Economy principle, the ONCs are prepared starting from the treatment of agriculture bagasse waste with ammonium persulfate – APS. This method permits to obtain ONCs fibers with rod or whisker shapes, with size and length in the range 6-10 nm and 90-150 nm, respectively. Ag-ONCs are then fabricated using a green photochemical approach. The UV irradiation works as radical initiator for the silver reduction, in water solution and at room temperature. The ONCs act as a template and reducing agent for silver nanoparticles formation, due to the specific hydroxyl and carboxyl groups on the cellulose surface. The structural and morphological properties of ONCs and Ag-ONCs nanocomposite are well evaluated by FT-IR, XRD, UV-Vis, AFM, SEM and TEM characterizations. The results showed that well crystalline, quasi-spherical silver nanoparticles of about 4-10 nm dispersed in the ONCs matrix are fabricated. Qualitative antibacterial tests towards gram negative (*Escherichia coli* and *Pseudomonas aeruginosa*) and gram positive (*Staphylococcus aureus* and *Bacillus subtilis*) bacteria are carried out and the results demonstrated that the Ag-ONCs inhibit the bacteria growth, with 12-14 mm of inhibition zone for both the bacteria groups. Also, quantitative antibacterial tests for *E. coli*, chosen as representative for its diffusion, are carried out and the bacteria growth rate and the inhibition rate for Ag-ONCs at different concentrations are evaluated. The analysis showed that the MIC (minimum inhibition concentration) for Ag is about 110µg/mL for *E.coli*. These results demonstrated that the Ag-ONCs possess suitable and promising antibacterial behavior and could be used for industrial and technological application.

Keywords: circular economy, nanocellulose, raw bagasse, silver nanoparticles, antibacterial properties

Declarations

Funding: The activities have been performed in the framework of the Joint Bilateral Agreement CNR/NRC (Italy/Egypt), Biennial Programme 2018-2019, for the project "Improvement of mechanical and barrier properties of biopolymer nano-composites for packaging applications".

Conflicts of interest/Competing interests: No conflict of interest exists.

Availability of data and material: (data transparency) 'Not applicable'

Code availability (software application or custom code) 'Not applicable'

Authors' contributions:

Daniela Caschera: Conceptualization, Methodology, Validation, Formal analysis, Investigation, Writing - original draft, Visualization. Funding acquisition **Abeer M. Adel:** Conceptualization, Methodology, Validation, Formal analysis, Investigation, Writing - review & editing, Funding acquisition. **Roberta G. Toro:** Investigation, Validation, Writing - review & editing. **Tilde de Caro:** Investigation,Validation. **Fulvio Federici:** Investigation. **Roberta Montanari:** Investigation, Validation. **Mona T. El- Shemy:** Methodology, Investigation, Validation.

1. Introduction

In the last years, many efforts have been carried out for the development of sustainable polymeric-based nanocomposites for several industrial applications (Kumar et al. 2020, Zinge and Kandasubramanian 2020, Jacob et al. 2018, Xiong et al. 2018). In particular, their sustainability, low cost and availability of large-scale commercial production have given to poly-saccharide materials, such as chitosan (Mohandas et al. 2018), starch (Abreu et al. 2015), and alginate (Esmat et al. 2017), a high priority in using them for emerging applications. In this context, cellulose, one of the most abundant natural polymers, has been intensively considered because its renewability, biodegradability and low cost (Tang et al. 2017, Kargarzadeh et al. 2018, Huang et al. 2019). Cellulose, a linear homopolymer of β-D 1, 4 glucose units, linked by glycoside bond, is made up of nanosized fibrils,

covered by lignin and hemicellulose. In particular, the nanocrystalline cellulose (NC) exhibits various remarkable properties, such as large surface area, high tensile strength and stiffness, suitable electrical and optical properties (Moon et al. 2011, Dufresne 2017). Furthermore, it can find application as suitable nano-filler for the fabrication of industrial nanocomposites and as an attractive bio template structure for the development of several nanomaterials (Adel et al 2017; Fortunati et al. 2014, Toro et al. 2020). In addition, thanks to the hydroxyl and carboxyl groups on its surface, NC can work as stabilization matrix for surfacting metallic nanoparticles, particularly Ag, Au, Ni, Pt and Pd nanoparticles (Hebeish et al. 2015; Kaushik and Moores 2016). However, NC can act not only as support, due to its high surface area and water suspend ability, promoting the nucleation of mono dispersed nanoparticles and preventing their agglomeration, but also as reducing agent for the metal precursors thanks to the presence of reductive hydroxyl groups on its surface (He et al. 2003). In recent years, a great effort has been taken on developing composites with cellulose and nano-sized inorganic compounds (El-Wakil et al. 2015, Herreros- López et al 2016, Jiao et al. 2018). Ag nanoparticles, in particular, have received great attention for their strong antibacterial activity at low concentrations. (Berndt et al 2013, Sharma et al. 2009; Martinez-Castanon et al. 2008). Different approaches have been evaluated for the fabrication of silver-NC based materials with antibacterial properties (Feng, et al. 2014, Errokh et al 2019). For example, Drogat et al. (2011) proposed the use of sodium periodate as oxidant for the ring opening in the cellulosic saccharide groups. In this way, the generation of aldehyde functionalities promoted the silver reduction thus producing Ag nanoparticles of about 35 nm in size. Li et al. (2015) instead showed the development of a novel solvent system for cellulose preparation, based on NaOH/urea aqueous solution pre-cooled to −12.5 °C. In this way, the following $AgNO_3$-cellulose composites with a low silver amount were prepared and their antibacterial properties were tested. Also, Zhang et al. (2019) presented a hydrothermal approach to obtain the formation of Ag nanoparticles on the surface of TEMPO-oxidized cellulose. Nevertheless, the specific chemical modification process, necessary to maximize the surface functionalities, could carry to the formation of several and more complex final co-products,

compromising the final properties of the cellulose itself and consequently the nanocomposite performances. With the aim to avoid the deterioration of the intrinsic properties of the cellulose during the complex chemical process required for metal salt reduction, the development of more green and simpler approaches to fabricate Ag-nanocellulose materials, even with high industrial scalability, is still urgently needed in consideration of their potential application in several industrial and technological fields.

For this purpose, here we propose a two-steps green procedure to fabricate a silver-carboxylated nanocellulose (Ag-ONCs) nanocomposite, starting from the nanocellulose extraction from waste materials, in accordance with the Circular Economy policy.

NCs can be extracted starting from different source of biomass, under moderate condition of acid or enzyme hydrolysis, to remove the amorphous regions (Xue et al 2017, García et al 2017). However due to the upraising challenges of raw materials scarcity, many efforts are exerted to find substituting materials which are more locally available, environmentally safer and cheaper (Bejoy et al. 2018). A potential candidate is the agriculture residue due to its high availability and characteristics (Sangeetha et al. 2017, Adel et al. 2018). Agriculture residues are produced in Egypt annually in huge amounts, and their recycling is considered a big add value to the Egyptian economy (Adel et al. 2016b). In this work, NCs are extracted from bagasse and they are opportunely oxidized in order to be used in biopolymer composites synthesis. Recently, ammonium persulfate (APS) has been proposed as a very efficient oxidant to produce carboxylated nanocellulose (ONCs) with high crystallinity and active carboxyl groups (Adel et al. 2017). Its specific properties, as high water solubility, low cost and commercially availability, permit it to be safely used on a large scale, presenting a low long-term toxicity lower than sodium and potassium counterparts, usually used in the cellulose extraction process (Vu et al. 2017). Therefore, using APS as oxidant agent leads to more homogeneous ONCs, without acid hydrolysis (Adel et al. 2017). This versatile procedure results to be particular attractive since it can be adopted to treat different cellulosic materials without the need for special pretreatments and in a relatively short time, to remove non-cellulosic plant contents (e.g. lignin and hemicellulose).

The as-produced ONCs have been then used as stabilizing/reducing matrix for silver precursor, in order to obtain Ag-ONCs nanocomposite. The formation of the metallic nanoparticles is normally achieved by treating the metallic salts with a reducing agent, ($NaBH_4$, hydrazine, PVP, Citric acid) in presence of a protective surfactant (Van Hyning et al. 2001; Sakai et al 2006; Caschera et al. 2009; Di Carlo et al. 2012). Nevertheless, the excessive amount of reducing agent required for the chemical reduction may be harmful to the environment and economy (Kitahama et al. 2014). In this view, the development of more environmental friendly chemistry processes is highly appealing, considering the urgent need for the minimization/elimination of waste and the adoption of more sustainable approaches. Here, compared with the previous studies cited above, we propose a green approach for the formation of Ag nanoparticles, based on UV irradiation, at room temperature, as radical initiator of the reducing process. Photo-reduction is a safer and more simple method respect to classic chemical reduction process, for which little or even no additional reducing agents are required (Coronato Courrol et al. 2007, Pal et al. 2017, Yang et al. 2017). Furthermore, the ONCs act as bio-template, instead of using organic solvents and/or hazardous reducing agents. A complete structural, morphological and chemical-physical characterization of the extracted ONCs and of Ag-ONCs nanocomposite is performed to detect the crystal structure, the morphology and the optical properties. In addition, the inhibition growth of the Ag-ONCs suspension, towards gram positive and gram negative bacteria are investigated, demonstrating the promising antibacterial properties of the nanocomposite.

2. Materials and Methods

2.1 Chemicals

Ammonium persulfate - APS (ACS reagent, ≥ 98.0 %), sodium hydroxide - NaOH (reagent grade, 97 %), silver nitrate - $AgNO_3$ (ACS reagent, ≥ 99.0 %) are all acquired from Sigma-Aldrich. Double distilled water is used for the aqueous solutions. The raw bagasse fibers, from Egyptian agricultural waste, are kindly supplied from Quena Company for pulp and paper industry. The chemical compositions of bagasse fibers are determined with Tappi standard methods for the different

components: lignin 20.40 % (T-222 om-88), α-cellulose 41.50 % (T-203 cm-99), hemicellulose content 27.20 % (T-223 cm-84) and ash 1.80 % (T-211 om-02).

2.2 Preparation of carboxylated nanocellulose (ONCs)

Carboxylated nanocellulose (ONCs) are prepared by adding 1 g of raw bagasse fibers previously milled to ≈ 1 mm length, to 100 mL of concentration 1.5 M APS solution. The mixture is heated at 60 °C for 24 h under a continuous mechanical stirring to give a suspension of ONCs. The suspension is centrifuged at 12000 rpm for 10 min, then the clear solution is decanted, and ONCs pellet is washed with water. The aqueous ONCs solution is mixed for 5 min and then centrifuged again. The centrifugation/washing cycles are repeated until the solution conductivity was ≈ 5 μ S cm^{-1} (pH 4). 1M NaOH is added to the suspension, to prepare the sodium form of ONCs, until it reached pH 7, followed by washing/centrifugation with distilled water. ONCs suspensions are filtered in a sintered glass funnel No 1 before being lyophilized (Figure 1). The yields of the prepared ONCs are calculated as a percentage of the weight of the final lyophilized product divided by the initial weight of the bagasse and found to be 28.89 %.

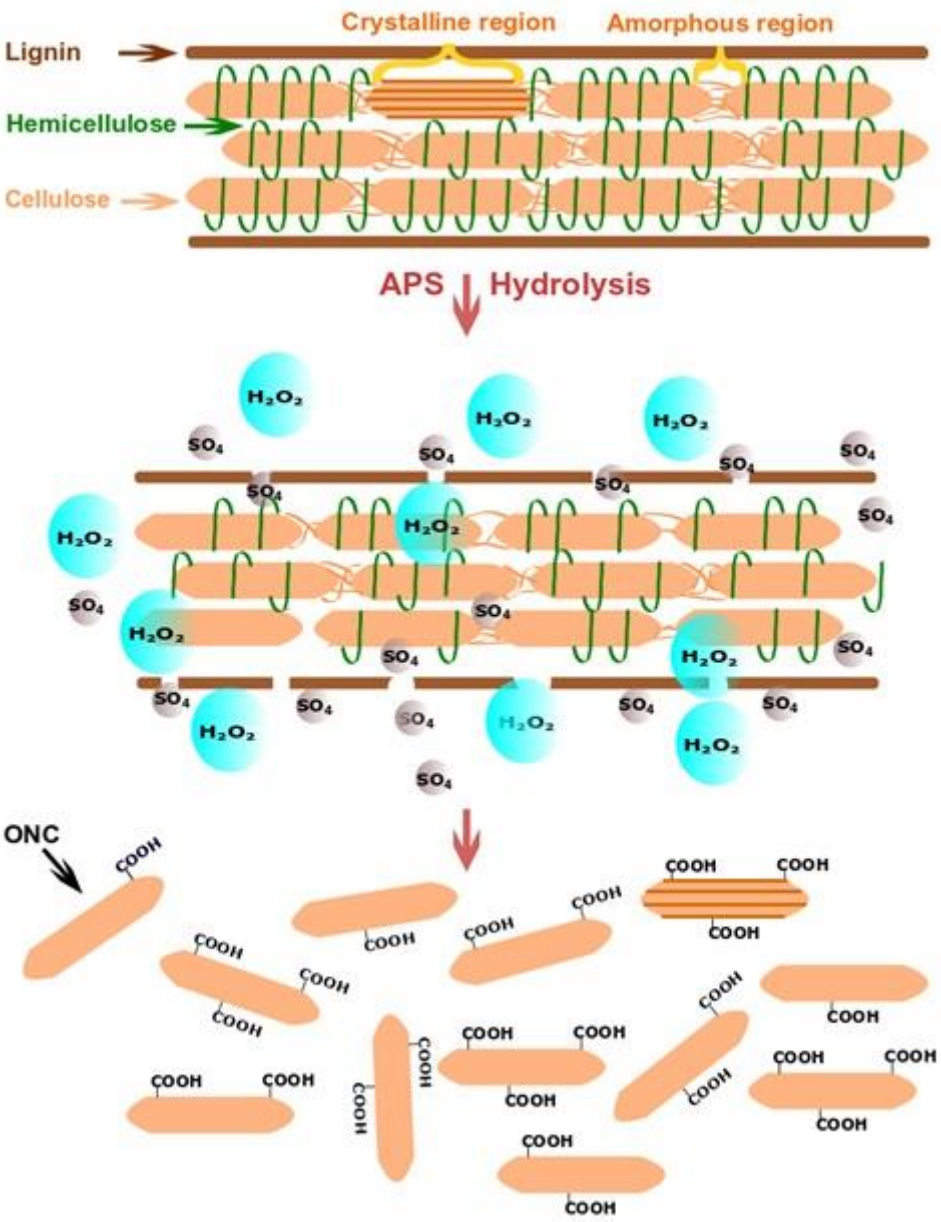

Fig. 1 Schematic representation for raw bagasse treated with aqueous APS

2.3 Preparation of Ag–ONCs by UV photoreduction

4 ml of the ONCs suspension (corresponding to about 46 mg) are opportunely diluted in the desired amount of distilled water, and then sonicated in an ice bath at 0 °C, for 5 min, to promote the dispersion. 12 ml of $AgNO_3$ solution (0.02 M) are added drop wise to the aqueous ONCs solution under magnetic stirring, at room temperature. The solution is stirred for 15 min, then it is put under UV lamp illumination (Spectroline® E-Series lamp bulb, Model EN-160, 6W, λ =365 nm) for 300

177 min. At the end, the initial transparent solution turned into a brownish color. Since the nanocellulose,
178 as reducing agent, is in great excess respect to Ag^+, then, the silver reduction is considered
179 quantitative and complete in the adopted experimental conditions and the nominal Ag concentration
180 of the as-obtained solution is about 0.3 mg/mL.

181 **2.4 Characterization methods of ONCs and Ag-ONCs nanocomposite solutions**

182 Zeta-potential analyses of ONCs are carried out on a Malvern Nano Zeta-sizer (Malvern, NanoZS,
183 UK) at 20 ± 0.1 °C. A field of 40 V is applied across the nominal electrode spacing of 16 mm. Before
184 measurements, the samples are ultrasonicated in a sonication bath for 2 min to increase particle
185 dispersibility. The average values are calculated from at least twelve runs.

186 Fourier-Transformed InfraRed (FTIR) spectra of raw bagasse fibers and lyophilized ONCs samples
187 are analyzed as KBr pellets (1 % cellulose in anhydrous KBr) on JASCO FTIR 6100 spectrometer
188 (Tokyo, Japan). Absorbance measurements are carried out in the range of 400–4000 cm^{-1}, with 60
189 scans and 4 cm^{-1} of resolution. The Degree of Oxidation (DO) is calculated by using the following
190 relationship (Habibi et al. 2006):

191 $$\mathbf{DO_{IR} = 0.01 + 0.7\ (I_{1715}/I_{1060})} \qquad \mathbf{(1)}$$

192 Where I_{1715}/I_{1060} is the ratio between absorption intensity of the FT-IR bands at 1715 and 1060 cm^{-1}.
193 Furthermore, the evaluation of the Degree of Oxidation (DO) of the ONCs was also performed using
194 conductometric titration, with a Jenway conductivity meter-4510 (UK), via the following equation
195 (Habibi et al. 2006):

196 $$DO = (162 \times V_{eq} \times C_{NaOH}) / (m - 36 \times V_{eq} \times C_{NaOH}) \qquad \mathbf{(2)}$$

197 where 162 g/mol is the molar mass of an anhydroglucose unit, V_{eq} is the amount of NaOH in mL at
198 the equivalent point, C_{NaOH} is the concentration (mol/L) and m is the weight of oven-dried ONCs (g).
199 The value of 36 corresponds to the difference between the molecular weight of an anhydroglucose
200 unit and that of the sodium salt of a glucuronic acid moiety.

201 Atomic Force Microscopy (AFM) is used for the morphological analysis of ONCs and Ag-ONCs, by
202 a Wet – SPM9600, (Shimadzu, Japan) operating in non-contact mode and also through a Dimension

3100, equipped with a Nano Scope IIIa, controller (Veeco, Santa Barbara, CA) operating in tapping mode.

Scanning Electron Microscopy (SEM) measurements are carried out using a Leo 1530 microscope (ZEISS), equipped with an Oxford 30 mm^2 SDD EDS and a KE Developments CENTAURUS detector, using the same parameter for both ONCs and Ag-ONCs sample (magnification 150.00K, EHT= 5kV). For both AFM and SEM measurements, the images are acquired depositing a drop of the solutions onto a glass slide and air-dried at room temperature to form a thin film.

Transmission Electron Microscope (TEM) of ONCs and Ag-ONCs nanocomposite are carried out using a JEOL JEM-2100 (Japan), in high resolution. Few drops of an aqueous 10 times diluted dispersion of the two samples are deposited on a micro grid, covered with a thin carbon film (≈200 nm). To enhance the microscopic resolution, the ONCs sample is stained with a 2 % uranyl acetate solution while Ag-ONCs are left without staining.

X-ray diffraction (XRD) of raw bagasse material, ONCs and Ag-ONCs samples are analyzed, in the range 2θ = 5–80°, by a Panalytical Empyrean X-ray diffractometer (PANalytical, Netherlands). The crystallinity index (CrI) is determined by Segal empirical equation:

$$\mathbf{Cr.I\ (\%) = [(I - I_{am})/I] \times 100} \qquad \mathbf{(2)}$$

Where I is the overall intensity of the (200) lattice peak at 2θ about 22.61°. I_{am} is intensity at 2θ about 18° for the amorphous material, where the intensity is minimum (Segal et al. 1959). The apparent crystallite sizes (L) and d-spaces between the crystals planes are calculated by the Debye-Scherrer equation:

$$\mathbf{L = K\,\lambda/\beta\,\cos\theta} \qquad \mathbf{(3)}$$

And the Bragg's law:

$$\mathbf{d = \lambda/2\,\sin\theta} \qquad \mathbf{(4)}$$

Where K = 0.94, λ = 0.1542 nm for Cu Ka radiation, β = half height width of the diffraction peak, and θ = Bragg angle of the most intense peak of the crystal, in case of Debye-Scherrer equation and all the lattice planes for Bragg's law, respectively.

UV-vis absorbance spectra of the Ag-ONCs are collected with a double beam spectrophotometer V-660 (Jasco), in the range 300–870 nm.

2.5 Antibacterial tests

The antibacterial examinations of prepared nanocomposites are carried out qualitatively and quantitatively. The qualitative test is accomplished through solid media (LB agar), using the agar diffusion disk method (AATCC Test Method 147-1988), while the quantitative test is done by using liquid media (LB Broth). The qualitative antibacterial activity of the nanocomposite is examined on four different bacterial species (*Bacillus subtilis* and *Staphylococcus aureus* as gram positive and *Escherichia coli* and *Pseudomonas aeruginosa* as gram negative). Blank paper disks (Schleicher & Schuell, Spain) with a diameter of 10 mm are soaked by 10 µL of the stock Ag-ONCs solution (nominal Ag_{conc} = 0.3 mg/mL), put on LB Agar, previously treated with the bacteria, and the corresponding inhibition zones have been estimated after 48 h, with slipping calipers of the National Committee for Clinical Laboratory Standards (M44-P. NCCLS, USA-2003).

The quantitative antibacterial activity of Ag-ONCs nanocomposites is evaluated for *E. coli*, chosen as representative bacteria. In this case, starting from the stock solution, solutions at different Ag concentration are prepared, (220, 110, 70 µg/mL) and 250 µL of each concentration is poured in to 50 ml of LB (solution). For the antibacterial test in liquid media freshly transformed *E. coli* are grown in LB medium to an OD_{590} of 0.6 and 5 µl of this solution are added to 50 ml of the Ag solutions and to the control (ONCs) for starting from a absorbance value (OD 590 nm) < 0.001. All samples are incubated at 37 °C for 24 h and the absorbance is measured at fixed intervals using the UV spectrophotometer (OD_{590nm}).

The growth curves obtained are used to evaluate the MIC (minimum inhibitory concentration) of Ag nanocomposites against *E. coli*. The minimum concentration of Ag necessary to inhibit the 83.3 % of bacteria is considered to be MIC.

253 The antibacterial efficiency of the nanocomposites with the different Ag amount is also compared by
254 evaluation of the relative inhibition rates. The inhibition rate is calculated as follows, measuring the
255 UV absorbance (OD) of the strain broth at 590 nm:

256 $$\textbf{Inhibition rate (\%)} = 100 - 100\,[(A_t - A_0)/(A_{con} - A_0)] \qquad (5)$$

257 with A_0 is the OD value of the culture broth before culture; A_t corresponds to the OD value of the test
258 sample while A_{con} represents the OD value of the mixed solution of broth and saline after incubation
259 for 24 h (Zhang et al. 2019).

260 **3. Results and Discussion**

261 **3.1. Morphological and chemical analysis of Carboxylated nanocellulose (ONCs)**

262 Eco-friendly ONCs from raw bagasse fibers are produced directly by APS one-pot treatment. Heating
263 the APS solution under acidic conditions favors the production of free radicals and hydrogen
264 peroxide, which allow the formation of the carboxylated nanocellulose ONCs, break down the
265 amorphous cellulose, and, at the same time, destroy the lignin and the other contaminants in the raw
266 materials (Cheng et al. 2014). Furthermore, the conversion/oxidation of the primary alcohol group at
267 C6 to the carboxylate form permits the site activation, favoring the nanometal fabrication.

268 The reaction mechanism for removing the non-cellulosic constituents (lignin, hemicellulose, pectin)
269 and the amorphous cellulosic regions involves two simultaneous processes. One is the free radicals
270 formation after the APS solution is heated ($S_2O_8^{2-}$ + heat→ $2SO_4^{\bullet -}$). The other comprises the
271 formation of hydrogen peroxide at low pH = 1 ($S_2O_8^{2-} + 2H_2O \rightarrow 2HSO_4^{\cdot -} + H_2O_2$). Free radicals
272 and H_2O_2 molecules are able to break down the aromatic rings of lignin, bleaching the raw bagasse
273 fibers, and penetrate through the cellulosic amorphous regions to form nanocellulose (Leung et al.
274 2011). Among the three main reactive hydroxyl groups, in each anhydro-glucose unit in a cellulose
275 polymer, the 6-OH is more susceptible to oxidation than the other two groups (2-OH and 3-OH),
276 leading to ONCs production with a degree of carboxylation of DO = 0.202 . The DO evaluation by
277 using the conductometric titration gives the very similar value of 0.195. In general, based on previous

studies, the APS oxidative treatment is selective, limited to the crystal surfaces and it does not influence the crystalline core of the whiskers (Habibi et al. 2006; Adel et al. 2018).

TEM, SEM and AFM (Figure 2a, b and c respectively) analyses are carried out to visualize the produced ONCs fibers. TEM image shows that the ONCs fibers appear as nanosized rod-shaped whiskers, bunched together into a tendon-like structure. The diameter of the fibers varies between 6-10 nm, while the length of the ONCs is about as 90-150 nm, also confirmed by SEM and AFM measurements (Figure 2b, c).

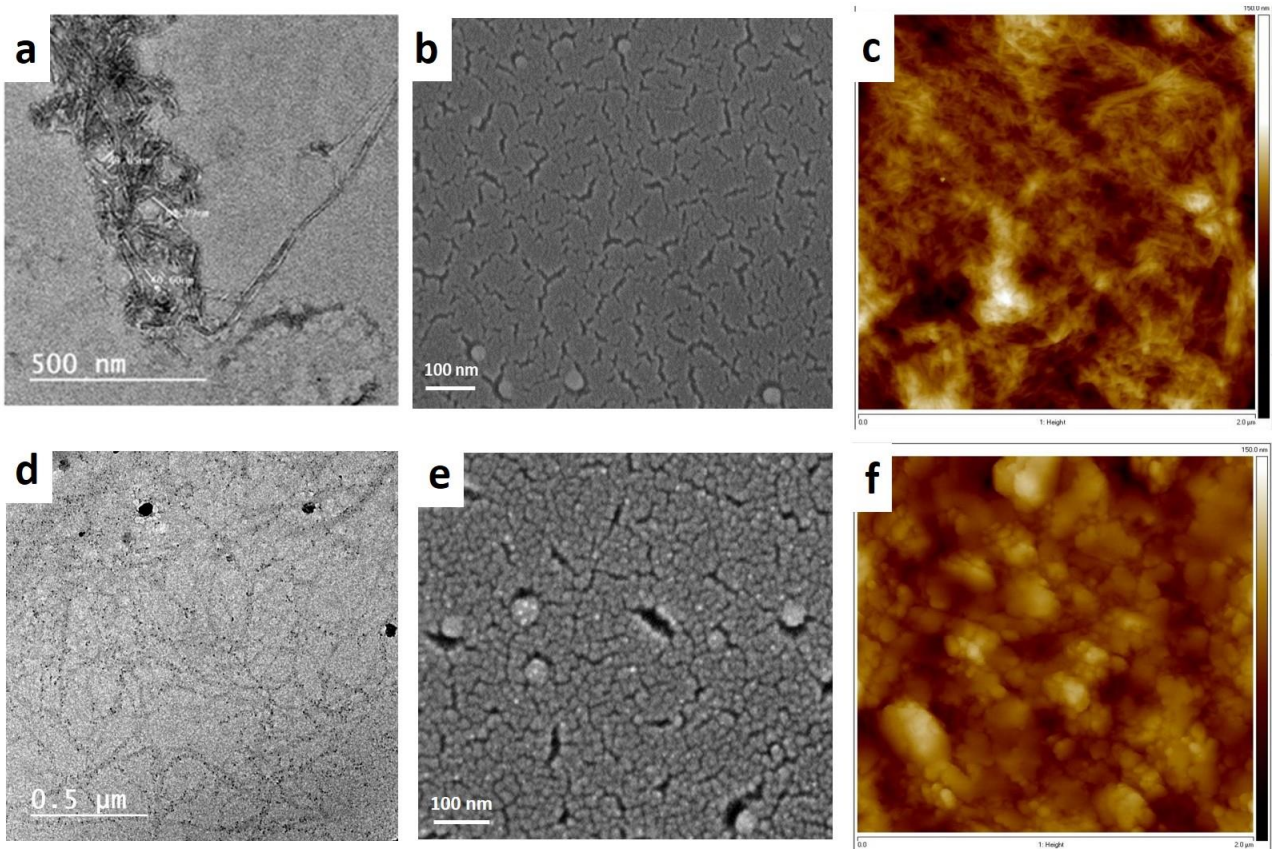

Fig. 2: (a) TEM, (b) SEM and (c) AFM micrograph for ONCs; (d) TEM, (e) SEM and (f) AFM of Ag-ONCs nanocomposite (300 min UV irradiation)

Zeta potential analysis is used to evaluate the stability of ONCs dispersions in aqueous media and the zeta potential value results to be −25 mV. The high dispersion stability of ONCs obtained by APS treatment is due to the negatively charged carboxylate groups present on the ONCs surface (Bondeson et al. 2006). Some agglomeration occurs, maybe due to the high hydrophilic nature of cellulose,

causing the aggregation during its drying (i.e., hornification). This problem could be avoided by balancing the hydrophilic–hydrophobic ratio and the adjustment of surface modeling (Habibi 2014; Mariano et al. 2014). When agglomeration occurs, the corresponding hydrodynamic diameter for ONCs is about 434 ± 125 nm, performed by dynamic light scattering (DLS) measurements, while zeta potential analysis confirms the value of -25 mV.

The clear influence of APS reaction on the chemical structure of raw bagasse fiber after hydrolysis to ONCs manifests itself in the corresponding FTIR spectrum as reported in Figure 3a.

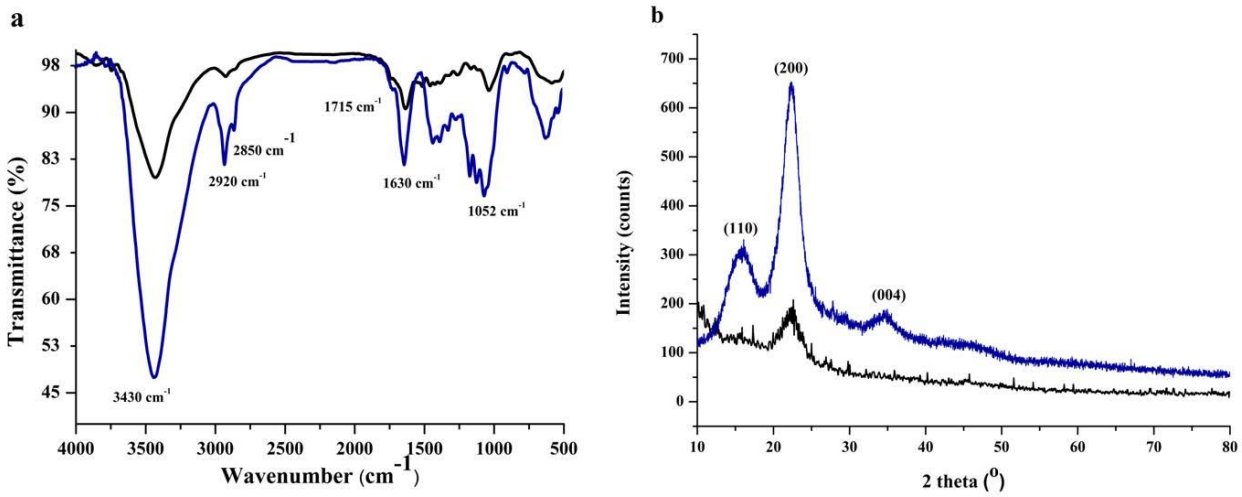

Fig. 3 (a) FTIR spectrum and (b) XRD profiles for — bagasse raw fibers and — ONCs

Not only new bands appear but also main cellulose fingerprint peaks intensities and positions are altered. The broad bands in the region between 3750 and 3100 cm^{-1} are attributed to the inter and intra hydrogen bonded O−H stretching vibrations, while the peaks at 2900 cm^{-1} and 2850 cm^{-1} correspond to stretching vibrations of the methyl groups. The characteristic features for the raw bagasse in the region 1700–850 cm^{-1} are attributed to its main constituents (lignin, hemicelluloses and α-cellulose). The bands around 1630 cm^{-1} correspond to the deformation vibration of adsorbed water molecules. The characteristic fingerprint bands of cellulose appear in the spectral region of 1500−800 cm^{-1}, assigned to the glucosidic ring vibrations of C−H, O−H, C=O and C−O−C (Adel et al. 2010; Shankar and Rhim 2016). The peak at 1715 cm^{-1} for ONCs could be assigned to C=O

valence vibration of COOH groups: the formation of the carboxyl groups through the oxidation of C6 primary hydroxyl groups by APS is also favored by the long interaction time between cellulose fibers and free radicals generated during the treatment (Leung et al. 2011). Moreover, from the enhancement of peak intensity at 1052 cm^{-1}, corresponding to –C-O-C- pyranose ring stretching, we can conclude that on APS treatment the cellulose content and crystallinity increase and pyranose ring remains intact.

Material	Lattice Plane	2 theta (°)	d-spacing (nm)	L (nm)	CrI
Raw bagasse	110*	15.87	0.5575	--	45.29
	200*	22.61	0.3927		
ONCs	110*	16.08	0.5503	5.0765	67.52
	200*	22.34	0.3973		
	004*	34.96	0.2563		
Ag-ONCs	110*	16.08	0.5503	4.6301	63.67
	200*	22.44	0.3956		
	004*	32.24	0.2772		
	110	38.12	0.2357	12.1460	
	200	43.72	0.2067		
	220	64.36	0.1445		
	311	77.72	0.1227		

Table 1 Lattice planes, 2 theta position, d-spacing, average crystallite sizes (L) and relative crystallinity index (CrI) of raw bagasse, ONCs and Ag-ONCs samples (* indicates the lattice planes - Miller indices- of cellulose crystal).

The XRD profiles of raw bagasse and ONCs fibers (Figure 3b) are determined to show the influence of APS hydrolysis on the crystalline structure of cellulose. The diffraction spectrum of raw bagasse presents a peak at about $2\theta = 22.61°$ and a broad signal at $2\theta = 15.87°$ with a relatively low crystallinity index ≈ 45.29. After reaction with APS solutions, the CrI of ONCs increases, becoming 49.08 % higher than that of the raw bagasse fibers. XRD of the ONCs fibers exhibits three diffraction

peaks fixed at 16.08° (110), 22.34° (200) and 34.96° (004) (Adel et al. 2016a). The crystalline form of bagasse fibers is not altered after the APS treatment but retains its original CI allomorph structure. The shift of diffraction peaks to higher 2-theta values and the enhancement of the crystallinity index upon oxidation-hydrolysis reactions are attributed to the disposal of non-cellulosic amorphous component in the raw material (extractives, lignin, hemicelluloses, etc) and to the rearrangement of cellulose into a more ordered and crystalline structure (Adel et al. 2016a).

3.2. Structural and morphological analysis of Ag-ONCs nanocomposite

The green proposed approach for the fabrication of Ag-ONCs nanocomposite is relied on the use of cellulose nanocrystals as a template to better control the UV silver reduction. Thanks to the electrostatic interaction between the abundant negative charge cellulosic OH/COOH groups in carboxylated cellulose nanocrystals and the positive Ag^+ ions, the ONCs can coordinate the metal nanoparticles, lowering the mobility of Ag^+ ions (Rehan et al. 2015), through ion−dipole interactions (Ifuku et al. 2009).

The reduction of Ag^+ to Ag^0 via the UV light exposure is indicated by a color change of the suspension from white-transparent to brown (Figure 4). Ag-ONCs formation is monitored by UV-Vis measurements (Figure 5) on the periodic sampling at the time interval of 5, 20, 60, 120, 180, 240 and 300 minutes, under UV lamp illumination (λ = 365 nm).

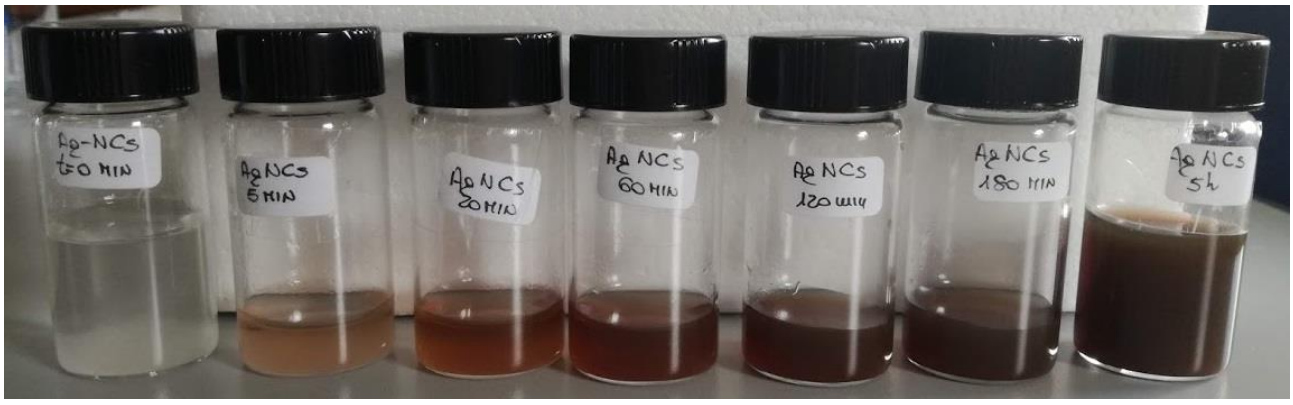

Fig. 4 Ag-ONCs suspension after different exposure time at UV light of 365 nm

Silver nanoparticles exhibit the characteristic plasmon absorption band in the visible region (400-500 nm). The starting suspension with ONCs and $AgNO_3$ (t = 0 min) shows no signals. After 5 minutes of UV irradiation, the UV−Vis spectrum of the Ag-ONCs suspension completely changes and it is possible to observe the appearance of a broad band at about 450 nm, as the contribution of the starting formation of Ag nanoparticles. Up to 120 minutes, the intensity at 450 nm increases linearly while, after 240 minutes of UV exposure, the formation of Ag-ONCs nanocomposite can be considered complete and quantitative, as no evolution of the UV-Visible spectra could be observed for longer exposition times.

The shoulder at 390-410 nm is indicative of the presence of smaller Ag clusters, while the broadness of the band could be due to the scattering of the suspension. The UV absorption band is also located in a relatively long-wavelength range, compared to the typical of AgNPs, generally observable at 410-430 nm. The red shift is normally associated to the presence of large size particles and a broad size distribution or some aggregation phenomena (Feng, et al. 2014; Xu et al. 2019). Nevertheless, TEM observation (Figure 2d) evidences the formation of well dispersed quite-spherical AgNPsin the ONCs matrix, with a diameter varied in a narrow range (4 - 10 nm). Also, SEM and AFM measurements (Figure 2e, f) confirm that the small AgNPs are uniformly and tightly attached to ONCs fibrils, that show a cauliflower-like agglomeration. In consideration of the small size of the Ag nanoparticles and their quite homogeneous distribution in the nanocellulose, the observed red shift and broadness of the SPR band could not be attributed exclusively to the presence of nanoparticles with different sizes. It is reported that the characteristic peak wavelength and broadening of the SPR for nanosystems can be also significantly influenced by the local dielectric environment around the particles, due to the presence of surface molecules (or functional groups) and capping agents, (Henglein and Giersing 1999; Suber et al. 2018). In this view, it is not possible to exclude that the stabilizing interaction between the AgNPs and the nanocellulose matrix could be a co-effect for the observed broadening and red shift.

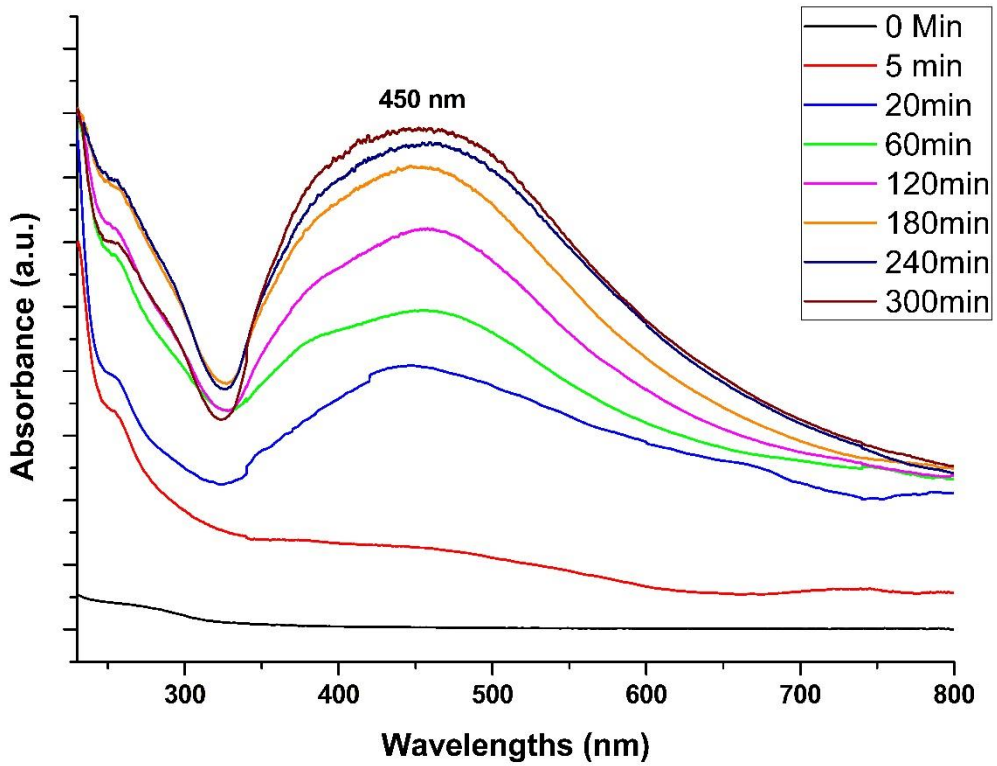

Fig. 5 UV-Vis spectra for the Ag-ONCs suspensions, collected after different UV exposure times

The UV irradiation can trigger the Ag^{+} ions reduction into Ag^{0}, permitting a better control in nanoparticles formation and growth (Jeong et al. 2014). The mechanism for silver reduction involves the oxidation of the end groups (hemiacetal) and alcoholic groups (CH_2OH) of the cellulose to produce carboxylic groups, maybe through some "radical intermediate" as suggested by Rehan et al (2017). Ag exhibits a well-known tendency to auto-catalytic reduction (Harada and Katagiri 2010) and Ag^{0} nanoparticles can act as center for the further reduction of silver ions. The Ag nuclei can coalesce to form higher silver clusters in absence of a stabilizing matrix (Emam and Ahmed 2016). In our case, the stabilization of the photo-reduction process and hence the prevention of AgNPs aggregation can be obtained thanks to the strong interaction between Ag and the cellulose surface groups (Hebeish et al. 2010; Atef et al. 2011).

Furthermore, since the silver reduction involves the oxidation of the alcoholic and/or aldehydic groups of the cellulose into carboxylic form, the increase of the carboxylic content of the cellulose fibers means that the redox reduction is running. To check this mechanism, the ATR-FTIR (Figure 6a) and XRD analysis (Figure 6b) of the Ag-ONCs nanocomposite obtained after 300 minutes of UV irradiation have been collected and compared with the results for the pure crystalline nanocellulose (ONCs) (Figure 3a,b).

From the comparison of FT-IR spectra, it is observable a relative decrease, in the Ag-ONCs, of the intensity of the band at 1630 cm^{-1} related to O-H bonds. Furthermore, the small shift in the hydrogen bond stretching vibration band from 3430 cm^{-1} to 3314 cm^{-1} in the Ag-ONCs could confirm the role of the OH groups in the formation and stabilization of the Ag nanoparticles (Hu et al. 2019). Also, the increase of the peaks intensity between 1100 cm^{-1} and 1020 cm^{-1}, especially the band at 1056 cm^{-1}, can be assigned to an increase of the oxidation degree of the cellulose, as the effect of its reducing role. These evidences could confirm the involving of carboxyl/hydroxyl cellulosic groups in the AgNPs formation and stabilization (Shankar et al. 2018).

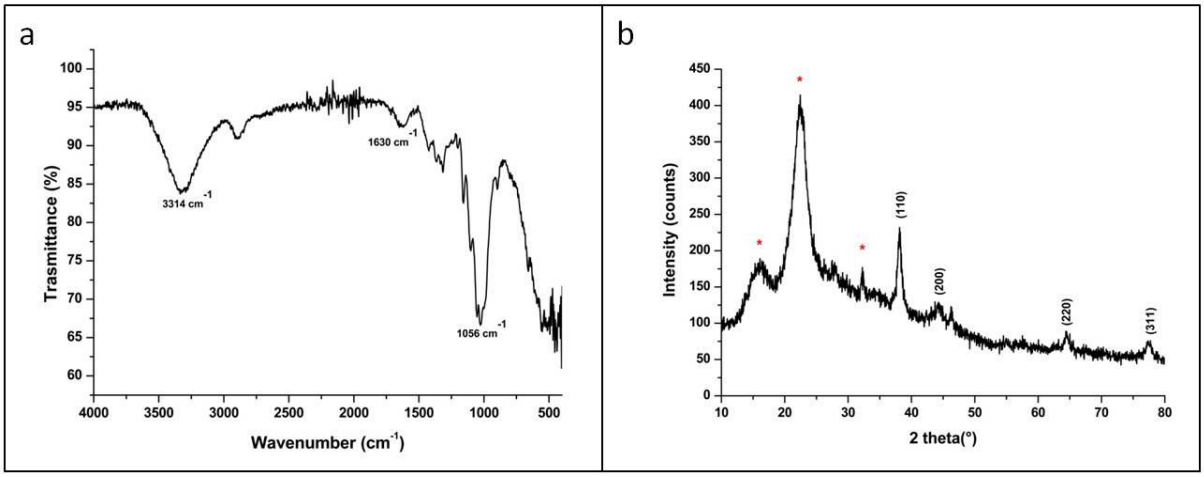

Fig. 6 Structural characterization for Ag-ONCs nanocomposite (after 300 min of UV irradiation) a) ATR_FT-IR measurements in the range 500-4000 cm^{-1}; b) XRD spectrum in the range 10-80°. The asterisks indicate the ONCs peaks

The X-ray diffraction pattern of Ag-ONCs (300 min UV irradiation) is shown in Figure 6b. The XRD still displays the strong reflections typical of crystalline cellulose and the typical Ag metallic diffraction peaks at 38.22° 44.77°, 64.43°, 77.44°, corresponding to (111), (200), (220) and (311) lattice planes for (FCC) Ag (JCPDS card no. 65-2871). No peaks related to the silver precursor are detectable in the spectrum, confirming the success of the metal reduction under the UV conditions. In particular, the presence of the silver peaks at $2\theta = 38.22°$ and 44.77° can be related to the presence of spherical or semi-spherical AgNPs structure (Yu et al. 2014), confirming the morphological analyses (see Figure 2d - f). Furthermore, it can be observed that both the crystallinity index and crystallite size of ONCs are reduced upon AgNPs production (Table 1). The same effects are observed when carboxymethyl cellulose has been complexed with different metal ions (Kaushik and Moores 2016). One explanation can arise from a possible rearrangement of the polymer chains which in turn changes the morphology of ONCs as a result of interaction with Ag ions (Hu et al 2019).

3.3 Antibacterial properties of Ag-ONCs nanocomposite

The qualitative antibacterial activity of the Ag-ONCs nanocomposite is examined on four different bacteria, *Bacillus subtilis* and *Staphylococcus aureus,* as gram positive, and *Escherichia coli* and *Pseudomonas aeruginosa,* as gram negative, by the disk diffusion method.

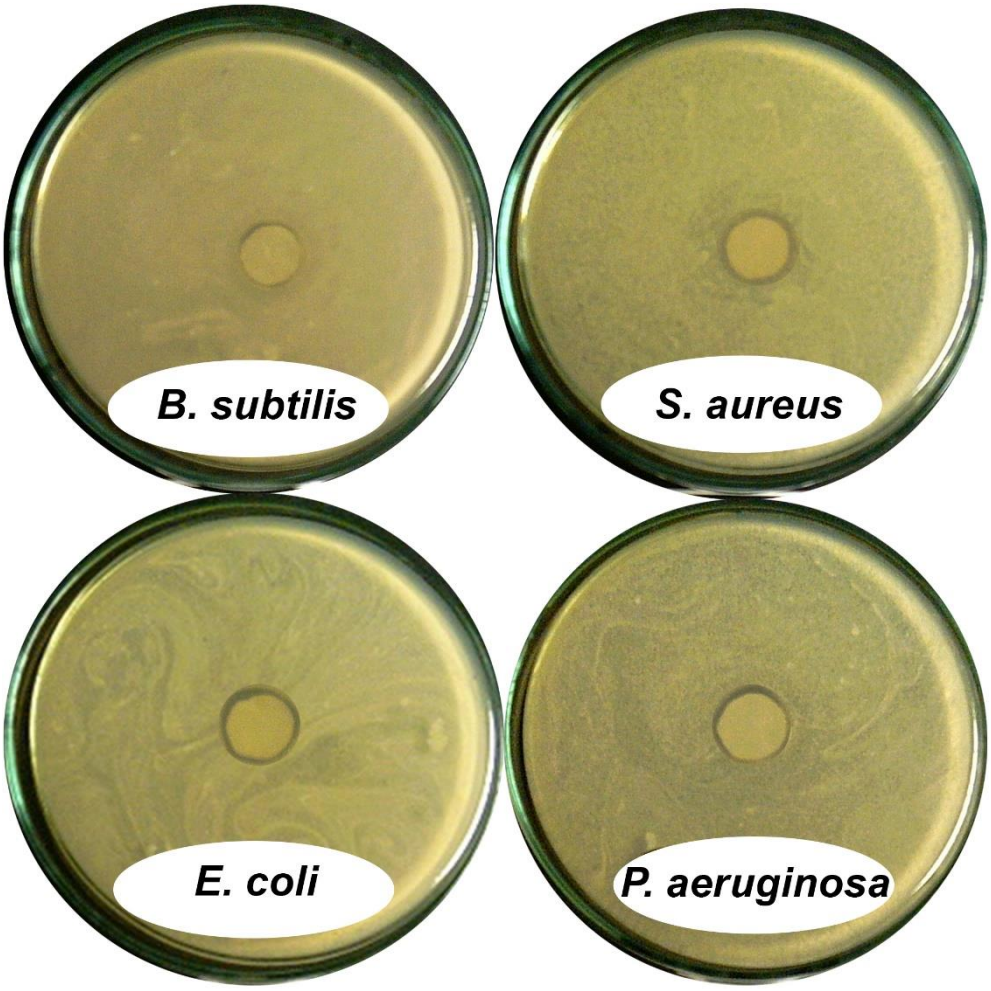

Fig. 7 The antimicrobial activity for Ag-ONCs nanocomposite versus different bacteria.

According to this method, a filter paper disc, soaked with the antibacterial chemical under test, is put on the agar broth with organism/bacteria placed on. The diffusion of the antibacterial material from the disc into the agar can take place only around the disc, and the bacteria growth will be inhibited in that area. This "no growth" area is called "**zone of inhibition**" or" **clear zone**". This agar-based method is a good alternative to broth-based methods because of its greater simplicity and speed in the use (Matar et al. 2003).

Figure 7 shows the antibacterial results of Ag-ONCs against *S. aureus, B. subtilis, E. coli and P. aeruginosa*. Ag-ONCs exhibit peculiar inhibition zones against all four bacteria, the corresponding diameter sizes of the inhibition zone are summarized in Table 2.

Nanocomposite sample	Inhibition zone diameter (mm/Sample)			
	Bacterial species			
	G^+		G^-	
	B. subtilis	***S. aureus***	***E. coli***	***P. aeruginosa***
Ag-ONCs	12	14	14	13

Table 2 Diameter size of the inhibition zone for Ag-ONCs nanocomposites through different bacteria.

The results show that the Ag-ONCs nanocomposites have a good antibacterial activity against *S. aureus, B. subtilis, E. coli and P. aeruginosa* and no substantial differences can be recognize for different bacteria. This evidence may be due to the great amounts of different functionalities on the cellulosic surface, which permits to the AgNPs to better interact with the cell surface of different bacteria (Ruparelia et al. 2008). Nevertheless, the size of the inhibition zone observed for Ag-ONCs nanocomposites is slightly smaller than that reported for other similar Ag-cellulose composites (Feng, et al. 2014; Xu et al. 2019). Since the size of the inhibition zone is strongly affected by the solubility and the molecular size of the antibacterial material, in our case, the lower size of the "clear zone" could be attributed to the low solubility of the Ag-ONCs that can limit the diffusion of the Ag antibacterial agent in the agar media.

For a quantitative evaluation of the antibacterial behavior of the Ag-ONCs nanocomposites, *E. coli* is chosen as representative class of bacteria for its diffusion in several contaminated environments. The growth curves for *E. coli* in presence of Ag-ONCs at different Ag concentrations are recorded, measuring the OD_{590nm} data every 3 h for 24 h. The results are shown in Figure 8a.

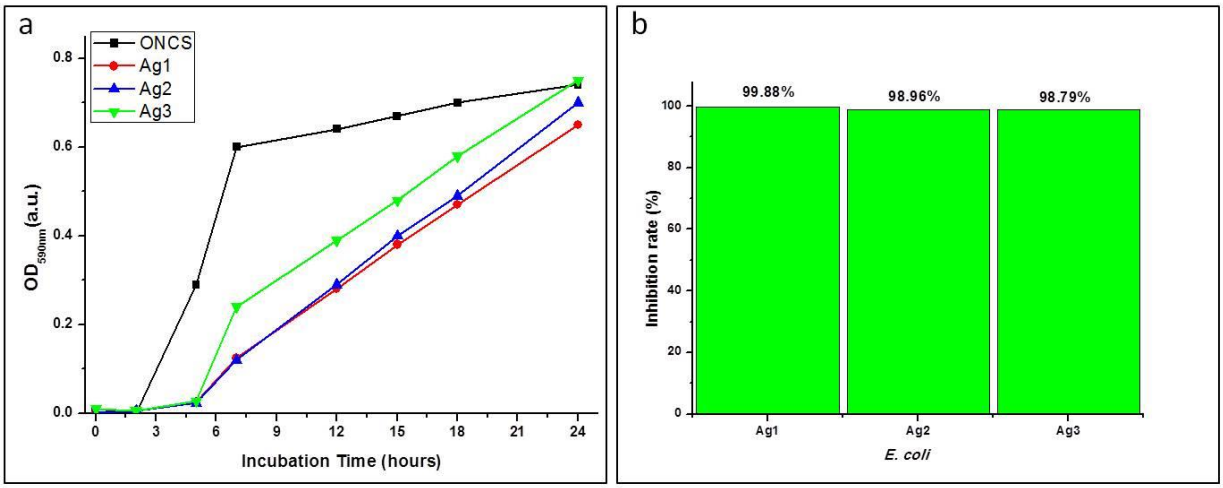

Fig. 8 (a) Bacterial Growth rate curves of E. coli, incubated for 24 h with ONCs (as control) and Ag-ONCs nanocomposites at 220 µg/mL (Ag1), 110 µg/mL (Ag2) and 70 µg/mL (Ag3); (b) Inhibition rate of the Ag-ONCs nanocomposites with different amount of Ag against *E. coli*.

As expected, the higher is the Ag concentration in the cellulosic nanocomposite; the lower is the *E. coli* bacteria growth. After 24 h, the entire Ag-ONCs nanocomposites reach a growth value very close to the ONCs-*E.coli* alone. Nevertheless, their increase is visibly more attenuate respect to the control. The MIC of the Ag-ONCs nanocomposites results to be 110 (µg/mL), a value well comparable to values reported in literature for similar Ag cellulosic-based nanocomposites (Shaheen and Fouda 2018), confirming the good promising antibacterial behavior of these systems.

The inhibition ratio of the Ag-ONCs with the different amount of Ag is also compared (Figure 8b), demonstrating the increasing of the bactericide effects with the increasing the amount of Ag.

4. Conclusion

In this study, silver-carboxylated nanocellulose (Ag-ONCs) nanocomposite is synthesized by a two-steps green method, taking into consideration the basin principle of the Circular Economy approach. Firstly, oxidized cellulose nanocrystals (ONCs) are obtained extracting the raw cellulose from the bagasse derived from Egyptian agricultural waste. The use of APS as oxidizing agent permits milder and more environmental friendly reaction conditions. Then, the ONCs are employed as template/reducing agent for AgNPs formation, by UV photoreduction. The obtained Ag-ONCs nanocomposites are analysed by UV–Vis, FTIR, XRD, AFM, SEM and TEM measurements. FTIR and XRD analyses confirmed the success of the Ag-ONCs nanocomposite formation, with high crystallinity. Morphological observations revealed that the Ag-ONCs have a quite-spherical form, 4-10 nm in size, firmly attached on the nanocellulose templates. The antibacterial tests indicated that the Ag-ONCs nanocomposite possesses a promising bactericidal efficiency against both gram positive and gram negative bacterial species and can be considered a good candidate as starting material for antibacterial applications in food packaging industries.

References

A. S. Abreu, M. Oliveira, A. Sá, R. M. Rodrigues, M. A. Cerqueira, A. A.Vicente, A.V. Machado 2015 Antimicrobial nanostructured starch based films for packaging. Carbohyd. Polym. 129 (20), 127-134. https://doi.org/10.1016/j.carbpol.2015.04.021

Adel A.M., Ahmed E.O., Ibrahim M.M., El-Zawawy W.K., Dufresne A. 2016a. Microfibrillated cellulose from agricultural residues. Part II: Strategic evaluation and market analysis for MFCE30. Ind Crops Prod 93, 175–185. https://doi.org/10.1016/j.indcrop.2016.04.042

Adel M. A., El-Gendy A.A., Mohamed D. A., Abou-Zeid R. E., El-Zawawy W. K., Dufresne A. 2016b. Microfibrillated cellulose from agricultural residues. Part I: Papermaking application. Ind Crops Prod 93, 161–174. https://doi.org/10.1016/j.indcrop.2016.04.043

494 Adel A.M., El-Shafei A., Ibrahim A., Al-Shemy M.T. 2018. Extraction of oxidized nanocellulose
495 from date palm (Phoenix Dactylifera L.) sheath fibers: Influence of CI and CII polymorphs on the
496 properties of chitosan/bionanocomposite films. Ind Crops Prod 124, 155–165.
497 https://doi.org/10.1016/j.indcrop.2018.07.073
498 Adel A.M., El-Shafei A., Al-Shemy M.T., Ibrahim A., Rabia A. (2017) Influence of cellulose
499 polymorphism on tunable mechanical and barrier properties of chitosan/oxidized nanocellulose bio-
500 composites. Egypt J Chem. 60, (4), 639-652. https://doi.org/10.21608/ejchem.2017.1194.1062
501 Adel A.M., El-Wahab Z.H.A., Ibrahim A.A., Al-Shemy M.T. 2010. Characterization of
502 microcrystalline cellulose prepared from lignocellulosic materials. Part I. Acid catalyzed hydrolysis.
503 Bioresour. Technol. 101, 124446–124455. https://doi.org/10.1016/j.biortech.2010.01.047
504 Atef A.I., Adel A.M., Abd El–Wahab Z.H., Al–Shemy M.T. 2011. Utilization of carboxymethyl
505 cellulose based on bean hulls as chelating agent. Synthesis, characterization and biological activity
506 Carbohydrate polymers 83, (1), 94-115. https://doi.org/10.1016/j.carbpol.2010.07.026
507 Bejoy T., Midhun C. R., Athira K. B, Rubiyah M. H., Jithin J., Moores A., Drisko G. L., Sanchez C.
508 2018, Nanocellulose, a Versatile Green Platform: From Biosources to Materials and Their
509 Applications Chem. Rev. 118, (24), 11575–11625 https://doi.org/10.1021/acs.chemrev.7b00627
510 Berndt S., Wesarg F., Wiegand C., Kralisch D., Müller F.A. 2013 Antimicrobial porous hybrids
511 consisting of bacterial nanocellulose and silver nanoparticles Cellulose 20, 771–783
512 https://doi.org/10.1007/s10570-013-9870-1
513 Bondeson D., Mathew A., Oksman K. 2006. Optimization of the isolation of nanocrystals from
514 microcrystalline cellulose by acid hydrolysis. Cellulose. 13,(2), 171–180.
515 https://doi.org/10.1007/s10570-006-9061-4
516 Caschera D., Federici F., Focanti F., Curulli A., Zane D., Padeletti G. 2009. Gold Nanoparticles -
517 modified GC Electrodes: electrochemical behaviour dependence of different neurotransmitters and
518 molecules of biological interest on the size and the shape of the particles. J. Nanop. Res. 11, 1925-
519 1936. https://doi.org/10.1007/s11051-008-9547-0

520 Cheng M., Qin Z., Liu Y., Qin Y., Li T., Chen L., Zhua M. 2014. Efficient extraction of carboxylated
521 spherical cellulose nanocrystals with narrow distribution through hydrolysis of lyocell fibers by using
522 ammonium persulfate as an oxidant. J Mater Chem A 2,(1), 251–258
523 https://doi.org/10.1039/C3TA13653A
524 Coronato Courrol L., Rodrigues de Oliveira Silva F., Gomes L. 2007. A simple method to synthesize
525 silver nanoparticles by photo-reduction. Coll. Surf A: Physicochem. Eng. Aspects 305, 54-57.
526 https://doi.org/10.1016/j.colsurfa.2007.04.052
527 Di Carlo G., Curulli A., Toro R.G., Bianchini C., de Caro T., Padeletti G., Zane D., Ingo G. M. 2012.
528 Green synthesis of gold-chitosan nanocomposites for caffeic acid sensing. Langmuir 28, 5471−5479.
529 https://doi.org/10.1021/la204924d
530 Drogat N., Granet R., Sol V., Memmi A., Saad N., Klein Koerkamp C., Bressollier P., Krausz P.
531 2011. Antimicrobial silver nanoparticles generated on cellulose nanocrystals. J. Nanopart. Res. 13,
532 1557-1562. https://doi.org/10.1007/s11051-010-9995-1
533 Dufresne A. 2017 Nanocellulose: From Nature to High Performance Tailored Materials Ed. Walter
534 de Gruyter GmbH & Co KG, ISBN 3110480417, 9783110480412
535 El-Wakil N. A., Hassan E. A., Abou-Zeid R. E., Dufresne A.2015 Development of wheat
536 gluten/nanocellulose/titanium dioxide nanocomposites for active food packaging. Carbohyd. Polym.
537 124, 337-346 https://doi.org/10.1016/j.carbpol.2015.01.076
538 Emam H., Ahmed H., 2016. Polysaccharides templates for assembly of nanosilver. Carbohyd.
539 Polym., 135, 300–307. http://dx.doi.org/10.1016/j.carbpol.2015.08.095
540 Errokh A., Magnin A., Putaux J.-L., Boufi S. 2019 Hybrid nanocellulose decorated with silver
541 nanoparticles as reinforcing filler with antibacterial properties. Mater. Sci. Engineer. C 105, 110044
542 https://doi.org/10.1016/j.msec.2019.110044
543 Esmat M., Farghali A. A., Khedr M. H., El-Sherbiny I. M 2017 Alginate-based nanocomposites for
544 efficient removal of heavy metal ions. Inter.J. Biol. Macromol. 102, 272-283
545 https://doi.org/10.1016/j.ijbiomac.2017.04.021

546 Feng J., Shi Q., Li W., Shu X., Chen A., Xie X., Huang X. 2014 Antimicrobial activity of silver
547 nanoparticles in situ growth on TEMPO-mediated oxidized bacterial cellulose. Cellulose 21, 4557–
548 4567. http://dx.doi.org/10.1007/s10570-014-0449-2
549 Fortunati E., Rinaldi S., Peltzer M., Bloise N., Visai L., Armentano I., Jiménez A., Latterini L., Kenny
550 J.M. 2014. Nano-biocomposite films with modified cellulose nanocrystals and synthesized silver
551 nanoparticles. Carbohydr. Polym. 101, (1), 1122–1133.
552 https://doi.org/10.1016/j.carbpol.2013.10.055
553 García A., Labidi J., Belgacem M. N., Bras J. 2017 The nanocellulose biorefinery: woody versus
554 herbaceous agricultural wastes for NCC production Cellulose 24, 693–704
555 https://doi.org/10.1007/s10570-016-1144-2
556 Habibi Y. 2014. Key advances in the chemical modification of nanocelluloses. Chem Soc Rev 43,
557 (5), 1519–1542. https://doi.org/10.1039/C3CS60204D
558 Habibi Y., Chanzy H., Vignon MR. 2006. TEMPO-mediated surface oxidation of cellulose whiskers.
559 Cellulose 13, (6), 679–687. https://doi.org/10.1007/s10570-017-1319-5
560 Harada M., Katagiri E. 2010. Mechanism of silver particle formation during photoreduction using in
561 situ time-resolved SAXS analysis. Langmuir 26, (23), 17896-17905.
562 https://doi.org/10.1021/la102705h
563 He J., Kunitake T., Nakao A. 2003. Facile In Situ Synthesis of Noble Metal Nanoparticles in Porous
564 Cellulose Fibers. Chem. Mater. 15, (23), 4401-4406. https://doi.org/10.1021/cm034720r
565 Hebeish A., Farag S., Sharaf S., Shaheen T.I. 2015. Nanosized carbamoylethylated cellulose as novel
566 precursor for preparation of metal nanoparticles. Fibers Polym. 16, (2), 276–284.
567 https://doi.org/10.1007/s12221-015-0276-6
568 Hebeish A., El-Rafie M., Abdel-Mohdy F., Abdel-Halim E., Emam H., 2010. Carboxymethyl
569 cellulose for green synthesis and stabilization of silver nanoparticles. Carbohyd Polym, 82, 933–941.
570 https://doi.org/10.1016/j.carbpol.2010.06.020

571 Henglein A., Giersing M. 1999. Formation of colloidal silver nanoparticles: capping action of citrate.
572 J Phys Chem B 103, 9533-9539. https://doi.org/10.1021/jp9925334
573 Herreros- López A., Hadad C., Yate L., Alshatwi A. A., Vicentini N., Carofiglio T., Prato M.
574 2016 Synthesis and Catalytic Activity of Gold Nanoparticles Supported on Dendrimeric
575 Nanocellulose Hybrids, Europ. J. Org. Chem. 19, 3186-3192 https://doi.org/10.1002/ejoc.201600148
576 Hu H., Wu X., Wang H., Wang H., Zhou J. 2019. Photo-reduction of Ag nanoparticles by using
577 cellulose-based micelles as soft templates: Catalytic and antimicrobial activities. Carbohyd Polym
578 213, 419–427. https://doi.org/10.1016/j.carbpol.2019.02.062
579 Huang J., Dufresne A., Lin N. 2019 Nanocellulose: From Fundamentals to Advanced Materials Ed.
580 John Wiley & Sons, ISBN 3527342699, 9783527342693
581 Ifuku S., Tsuji M., Morimoto M., Saimoto H., Yano H. 2009 Synthesis of Silver Nanoparticles
582 Templated by TEMPO-Mediated Oxidized Bacterial Cellulose Nanofibers. Biomacromol 10, (9),
583 2714-2717. https://doi.org/10.1021/bm9006979
584 Jacob J., Haponiuk J. T., Thomas S., Gopi S. 2018 Biopolymer based nanomaterials in drug delivery
585 systems: A review. Mat. Today Chem. 9, 43-55 https://doi.org/10.1016/j.mtchem.2018.05.002
586 Jeong L., Park W.H. 2014. Preparation and Characterization of Gelatin Nanofibers Containing Silver
587 Nanoparticles. Inter J Mol Sci 15, 6857-6879. https://doi.org/10.3390/ijms15046857
588 Jiao L., Li Q., Deng J., Okosi N., Xia J., Su M. 2018 Nanocellulose templated growth of ultra-small
589 bismuth nanoparticles for enhanced radiation therapy Nanoscale 10, 6751-6757
590 https://doi.org/10.1039/C7NR06462D
591 Kargarzadeh H., Mariano M., Gopakumar D., Ahmad I., Thomas S., Dufresne A., Huang J., Lin N.
592 2018 Advances in cellulose nanomaterials Cellulose 25 (4), 2151-2189
593 https://doi.org/10.1007/s10570-018-1723-5
594 Kaushik M., Moores A. 2016. Review: nanocelluloses as versatile supports for metal nanoparticles
595 and their applications in catalysis. Green Chem 18, (3), 622–637.
596 https://doi.org/10.1039/C5GC02500A

597 Kitahama Y., Ikemachi T., Suzuki T., Miura T., Ozaki Y. 2014. Plasmonic properties of triangle-
598 shaped silver trimers selectively fabricated by near-field photo-reduction using an apertured
599 cantilever for an atomic force microscope. Chem Comm, 50, 9693-9696.
600 https://doi.org/10.1039/C4CC04230A
601 Kumar S., Mukherjee A., Dutta J. 2020 Chitosan based nanocomposite films and coatings: Emerging
602 antimicrobial food packaging alternatives. Trends Food Sci. Technol. 97, 196-209
603 https://doi.org/10.1016/j.tifs.2020.01.002
604 Leung A.C.W., Hrapovic S., Lam E., Liu Y., Male K.B., Mahmoud K.A., Luong J. H. T. 2011.
605 Characteristics and properties of carboxylated cellulose nanocrystals prepared from a novel one-step
606 procedure. Small. 7,(3), 302–305. https://doi.org/10.1002/smll.201001715
607 Li R., He M., Li T., Zhang L. 2015. Preparation and properties of cellulose/silver nanocomposite
608 fibers. Carbohydr. Polym 115, 269-275. https://doi.org/10.1016/j.carbpol.2014.08.046
609 Mariano M., El Kissi N., Dufresne A. 2014. Cellulose nanocrystals and related nanocomposites:
610 Review of some properties and challenges. J Polym Sci Part B Polym Phys. 52, (12), 791–806.
611 https://doi.org/10.1002/polb.23490
612 Martínez-Castañón G. A., Niño-Martínez N., Martínez-Gutierrez F., Martínez-Mendoza J. R., Ruiz
613 F. 2008. Synthesis and antibacterial activity of silver nanoparticles with different sizes. J. Nanop.
614 Res. 10, (8), 1343–1348. https://doi.org/10.1007/s11051-008-9428-6
615 Matar M.J., Ostrosky-Zeichner L., Paetznick V. L., Rodriguez J. R., Chen E., Rex J. H. 2003.
616 Correlation between E-test, disk diffusion, and microdilution methods for antifungal susceptibility
617 testing of fluconazole and voriconazole. Antimicrob. Agents Chemother. 47, 1647–1651.
618 https://doi.org/10.1128/AAC.47.5.1647–1651.2003
619 Mohandas A., Raja S. D., Jayakumar B. R. 2018 Chitosan based metallic nanocomposite scaffolds as
620 antimicrobial wound dressings. Bioactive Mater. 3 (3), 267-277

621 Moon R.J., Martini A., Nairn J., Simonsen J., Youngblood J. 2011. Cellulose nanomaterials review:
622 structure, properties and nanocomposites. Chem. Soc. Rev. 40, 3941-3994.
623 https://doi.org/10.1039/C0CS00108B
624 Pal S., Nisi R., Stoppa M., Licciulli A. 2017 Silver-Functionalized Bacterial Cellulose as
625 Antibacterial Membrane for Wound-Healing Applications. ACS Omega 2 (7), 3632–3639 https://doi:
626 10.1021/acsomega.7b00442.
627 Rehan M., Barhoum A., Van Assche G., Dufresne A., Gatjen L., Wilken R. 2017. Towards
628 multifunctional cellulosic fabric: UV photo reduction and in situ synthesis of silver nanoparticles into
629 cellulosic fabrics. Intern. J. Biol. Macromol. 98, 877-866.
630 https://doi.org/10.1016/j.ijbiomac.2017.02.058
631 Rehan M., Mashaly H.M., Mowafi S., Bou El-Kheir A., Emam H.E. 2015. Multi-functional textile
632 design using in-situ Ag NPs incorporation into natural fabric matrix. Dyes Pigm. 118, 9-17.
633 https://doi.org/10.1016/j.dyepig.2015.02.021.
634 Ruparelia J.P., Chatterjee A.K., Duttagupta S.P., Mukherji S., 2008. Strain specificity in antimicrobial
635 activity of silver and copper nanoparticles. Acta Biomater. 4, 707–716.
636 https://doi.org/10.1016/j.actbio.2007.11.006
637 Sangeetha J., Thangadurai D., Hospet R., Purushotham P., Manowade K. R., Mujeeb M. A.,
638 Mundaragi A. C., Jogaiah S., David M., Thimmappa S. C., Prasad R., Harish E. R. 2017 Production
639 of Bionanomaterials from Agricultural Wastes In: Nanotechnology Prasad R., Kumar M., Kumar V.
640 (eds) Springer, Singapore pp 33-58 https://doi.org/10.1007/978-981-10-4573-8_3
641 Sakai H., Kanada T., Shibata H., Ohkubo T., Abe M. 2006. Preparation of highly dispersed core/shell-
642 type titania nanocapsules containing a single Ag nanoparticles. J. Am. Chem Soc. 128, 4944-4945.
643 https://doi.org/10.1021/ja058083c
644 Segal L., Creely J.J.,. Martin Jr A.E, Conrad C.M.C. 1959. An Empirical Method for Estimating the
645 Degree of Crystallinity of Native Cellulose Using the X-Ray Diffractometer. Text Res J. 29, 786–
646 794. https://doi.org/10.1177/004051755902901003

647 Shaheen T.I., Fouda A. 2018. Green approach for one-pot synthesys of silver nanorods using cellulose
648 nanocrystal and their cytoxicity and antibacterial assessment. Int J Biol Macromol 106, 784-792.
649 https://doi.org/10.1016/j.ijbiomac.2017.08.070
650 Shankar S., Oun A. A., Rhim J-W. 2018. Preparation of antimicrobial hybrid nano-materials using
651 regenerated cellulose and metallic nanoparticles. Inter. J Biol. Macromol. 107, 17-27.
652 https://doi.org/10.1016/j.ijbiomac.2017.08.129
653 Shankar S., Rhim J.W. 2016. Preparation of nanocellulose from micro-crystalline cellulose: The
654 effect on the performance and properties of agar-based composite films. Carbohydr Polym. 135, 18–
655 26. https://doi.org/10.1016/j.carbpol.2015.08.082
656 Sharma V.K., Yngard R.A., Lin Y. 2009. Silver nanoparticles: Green synthesis and their antimicrobial
657 activities. Adv Colloid Interface Sci 145, (1), 283–296. https://doi.org/10.1016/j.cis.2008.09.002
658 Suber L., Imperatori P., Pilloni L., Caschera D., Angelini N., Mezzi A., Kaciulis S., Iadecola A.,
659 Joseph B., Campi G. 2018. Nanocluster superstructures or nanoparticles? The self-consuming
660 scaffold decides. Nanoscale 10, 7472-7483. https://doi.org/10.1039/c7nr09520a
661 Tang J., Sisler J., Grishkewich N., Tam K.C. 2017. Functionalization of cellulose nanocystals for
662 advanced applications. J. Colloid Inter. Sci. 494, 397-409. https://doi.org/10.1016/j.jcis.2017.01.077
663 Toro R.G., Diab M., de Caro T., Al-Shemy M., Adel A., Caschera D. 2020 Study of the E
664 ect of Titanium Dioxide Hydrosol on the Photocatalytic and Mechanical Properties of Paper Sheets .
665 Materials 13, 1326; https://doi:10.3390/ma13061326
666 Van Hyning D., Klemperer W., Zucoski C. 2001. Silver nanoparticles formation: prediction and
667 verification of the aggregative growth model. Langmuir 17, 3128-3135.
668 https://doi.org/10.1021/la000856h
669 Vu N.D., Tran H. T., Bui N.D., Vu C.D., Nguyen H. V. 2017 Lignin and Cellulose Extraction from
670 Vietnam's Rice Straw Using Ultrasound-Assisted Alkaline Treatment Method. Inter. J. Polym. Sci.
671 Article ID 1063695, 8 pages https://doi.org/10.1155/2017/1063695

672 Xiong R., Grant A. M., Ma R., Zhang S., Tsukruk V. V. 2018 Naturally-derived biopolymer
673 nanocomposites: Interfacial design, properties and emerging applications. Mater. Sci. Eng.: R:
674 Reports 125, 1-41 https://doi.org/10.1016/j.mser.2018.01.002
675 Xu, Q., Jin, L., Wang, Y., Chen H., Qin M. 2019 Synthesis of silver nanoparticles using dialdehyde
676 cellulose nanocrystal as a multi-functional agent and application to antibacterial paper. Cellulose 26,
677 1309–1321. https://doi.org/10.1007/s10570-018-2118-3
678 Xue Y., Mou Z., Xiao H. 2017 Nanocellulose as a sustainable biomass material: structure, properties,
679 present status and future prospects in biomedical applications Nanoscale 9, 14758-14781
680 https://doi.org/10.1039/C7NR04994C
681 Yang G., Yao Y., Wang C. 2017 Green synthesis of silver nanoparticles impregnated bacterial
682 cellulose-alginate composite film with improved properties. Mater. Letters 209, 11-14
683 https://doi.org/10.1016/j.matlet.2017.07.097
684 Yu H-Y., Qin Z-.Y., Sun B., Feng Yan C., Yao J.-M. 2014. One-pot green fabrication and
685 antibacterial activity of thermally stable corn-like CNC/Ag nanocomposites. J Nanopart Res 16, 2202.
686 https://doi.org/10.1007/s11051-013-2202-4
687 Zhang X., Sun H., Tan S., Gao J., Fu Y., Liu Z. 2019. Hydrothermal synthesis of Ag nanoparticles
688 on the nanocellulose and their antibacterial study. Inorg. Chem. Commun. 100, 44-55.
689 https://doi.org/10.1016/j.inoche.2018.12.012
690 C. Zinge, Kandasubramanian B. 2020 Nanocellulose based biodegradable polymers, European
691 Polymer Journal 133, 109758 https://doi.org/10.1016/j.eurpolymj.2020.109758
692